J Therm Anal Calorim (2010) 99:931–938
DOI 10.1007/s10973-009-0640-0

# Lanthanide complexes of 3-methoxy-salicylaldehyde

## Thermal and kinetic investigation by simultaneous TG/DTG–DTA coupled with MS

**Christos Papadopoulos · Nikolaos Kantiranis · Stefano Vecchio · Maria Lalia-Kantouri**

MEDICTA2009 Special Issue


**Abstract** The reaction of a lanthanide(III) nitrate (Ln = Pr, Nd, Gd, Dy, Er) with 3-methoxy-salicylaldehyde(3-$OCH_3$-saloH), afforded neutral complexes of the general formula [Ln(3-$OCH_3$-salo)$_3$], which were characterized by means of elemental analysis, FT-IR spectra, TG-DTA curves, and magnetic measurements. The released products, due to the thermal decomposition were analyzed by on-line coupling MS spectrometer to the thermobalance in argon, allowed to prove the proposed decomposition stages. In order to confirm the stability scale provided on the basis of the onset decomposition temperature, a kinetic analysis of the three decomposition stages was made using the Kissinger equation, while the complex nature of the decomposition kinetics was revealed by the isoconvertional Ozawa–Flynn–Wall method.

**Keywords** Lanthanide(III) complexes · 3-Methoxy-salicylaldehyde · Coupled TG-MS · Decomposition kinetics · TG/DTG–DTA · PXRD

C. Papadopoulos · M. Lalia-Kantouri (✉)
Department of Chemistry, Laboratory of Inorganic Chemistry, Faculty of Sciences, Aristotle University of Thessaloniki, P.O. Box 135, Thessaloniki 54124, Greece
e-mail: lalia@chem.auth.gr

N. Kantiranis
Department of Mineralogy-Petrology-Economic Geology, Faculty of Sciences, Aristotle University of Thessaloniki, Thessaloniki 54124, Greece

S. Vecchio
Department of Chemical Engineering (I.C.M.A.), University of Rome, "La Sapienza", Via del Castro Laurenziano 7, 00161 Rome, Italy

## Introduction

Lanthanide complexes are of continuing interest mainly due to their structural and catalytic properties [1] and their applications in diagnostic pharmaceuticals [2] and laser technology [3, 4]. Besides, the strong coordinating properties of 2-hydroxy-phenones or 2-hydroxy-benzaldehydes (salicylaldehyde, saloH) and their derivatives with 3d transition metals have stimulated research in these compounds, which find applications in both pure [5] and applied chemistry fields, especially in extractive metallurgy as analytical reagents [6]. These ligands are known to coordinate in a bidentate manner with divalent transition metals in the mono-anionic form, adopting square-planar geometry, [Cu(5-Br-salo)$_2$] [7], [Fe(salo)$_2$] [8], or with vanadium octahedral arrangement [VO(3-$OCH_3$-salo)$_2$($H_2O$)] [9]. There is no reference of any salicylaldehyde or 2-hydroxy-phenone complex with trivalent 3d metal or trivalent lanthanides structurally characterized. It is recently found, however, by us that under proper conditions, 3-$OCH_3$-salicylaldehyde with Fe(III) ion can coordinate with two different modes and as bridging ligand, forming polynuclear complexes [$Fe_2$(3-$OCH_3$-salo)$_8$$Na_5$]8$H_2O$ [10], while 2-OH-benzophenones give the simple complexes [Fe(2-OH-benzophenone)$_3$] [11]. Recently, there is an increasing research interest on the thermal properties of the lanthanide complexes with ligands having O and/or N donor ability, studied by TG-DTA techniques [12–15].

In the course of our studies on the lanthanide chemistry [16, 17], we report here the synthesis, spectral (IR), and thermal studies (TG/DTG–DTA) of five new lanthanide complexes with the ligand 3-methoxy-salicylaldehyde (3-$OCH_3$-saloH). The evolved gaseous products from the thermal decomposition were analyzed by MS coupled on line with the TG to verify the decomposition mode.

The thermal stability cannot be assessed only on the basis of the decomposition temperature, since its value can be influenced by several operative conditions (i.e., sample mass, heating rate, atmosphere used, and its flux). On the other hand, some authors used kinetic analysis to provide stability scales of a series of lanthanide complexes, but they consider the activation energy only as a stability parameter [18, 19]. Actually, this procedure can be considered questionable since usually higher activation energies $E$ (which means high stability from an enthalpic point of view) are associated to higher pre-exponential factors $A$ (which correspond to lower stability from an entropic point of view). This problem can be overcome by considering the rate constant, obtained from the knowledge of both $E$ and $A$ values using the Arrhenius equation. In this study, a kinetic analysis was applied to the first three stages of decomposition to provide a stability scale comparing with the one constructed on the basis of the onset decomposition temperature.

## Experimental

The hydrated nitrate salts of lanthanide ($Ln(NO_3)_3{\cdot}xH_2O$, where Ln = Pr, Nd, Gd, Dy, Er) and the organic compound 2-hydroxy, 3-methoxy-benzaldehyde (3-methoxy-salicylaldehyde, commonly known as *o*-vanilline) were purchased as reagent grade from Aldrich and were used without further purification. All solvents were distilled prior to use.

### Synthesis of the complexes [Ln(3-methoxy-salicylaldehyde)$_3$]

[Ln(3-Methoxy-salicylaldehyde)$_3$] complexes were prepared by the following general procedure: to a water–ethanol solution (15 mL) of lanthanide nitrate (1 mmol) was added drop-wise a methanolic solution (25 mL) of the ligand 3-methoxy-salicylaldehyde (4 mmol), deprotonated by $CH_3ONa$. After 4 h stirring, microcrystalline yellow solids were obtained, filtered off, washed with small portions of ethanol, and dried in vacuum over anhydrous calcium chloride. The compounds are soluble in MeOH, $CH_2Cl_2$, DMF but virtually insoluble in $H_2O$, EtOH, and $Et_2O$.

### Instrumental methods

Stoichiometric analyses (C, H) were performed on a Perkin-Elmer 240B elemental analyzer. Metal content was determined by EDTA titration after decomposition with nitric acid using as indicator xylenol orange and buffer hexamethylenetetramine [20].

Magnetic susceptibility measurements on powdered samples were performed at 25 °C employing the Faraday method in a home build balance calibrated against $Hg[Co(SCN)_4]$. Molar conductivities were measured in DMF solutions, employing a WTW conductivity bridge and a calibrated dip-type cell. Infrared spectra were recorded on a Perkin-Elmer FT-IR 1650 spectrometer, in the region 4000–200 $cm^{-1}$ using KBr pellets. The simultaneous TG/DTG–DTA curves were obtained on a SETARAM thermal analyzer, model SETSYS-1200. The samples of approximately 10 mg were heated in platinum crucibles, in nitrogen atmosphere at a flow rate of 80 ml $min^{-1}$, within the temperature range 30–1000 °C. For the kinetic study of decomposition processes, the TG/DTG–DTA experiments were carried out at several heating rates (5, 10, 15, and 20 °C $min^{-1}$) using the isoconversional Ozawa–Flynn–Wall (OFW) [21, 22], which is based on Eq. 1:

$$\ln(\beta) = a + b(1/T_\alpha) \quad (1)$$

where $a = \ln[(A_\alpha{\cdot}E_\alpha)/R] - \ln g(\alpha) - 5.3305$ and $b = -1.052{\cdot}(E_\alpha/R)$ assuming that the Doyle's approximation [23] is valid over the entire range of $\alpha$. $E_\alpha$ and $T_\alpha$ are the activation energies and temperatures, respectively, calculated at each extent of reaction, $\alpha$, and $R$ is the gas constant. Once the conversion dependence on activation energy is established for each decomposition stage the Kissinger method [24] was applied, using Eq. 2:

$$\ln\left(\beta/T_m^2\right) = a' + b'(1/T_m) \quad (2)$$

where $a' = \ln[(A\ R)/E]$ and $b' = -E{\cdot}10^3/R$, $E$, and $A$ being the activation energy and pre-exponential factor associated to each decomposition stage, respectively. The kinetic parameters thus obtained were subsequently used to calculate the specific rate constant at the mean of the corresponding temperature range using the Arrhenius equation.

The thermal behavior was investigated using TG data at 10 °C $min^{-1}$. Mass spectra (MS) of the gaseous evolved moiety during the experiments were recorded since the TG apparatus was coupled with a Quadrupole Mass Spectrometer (QMS) model Thermostar. The TG was linked to a heated gas cell of the MS by means of a heated transfer line, at temperature 180 °C. Data were processed using online connected computer system with commercial software Quadstar. Powder XRD was performed using a Philips PW 1710 diffractometer with Ni-filtered CuK$\alpha$ radiation on randomly oriented samples. The samples were scanned within the range $2\theta$ = 5–80°.

## Results and discussion

The reaction of the lanthanide nitrate with the ligand 3-methoxy-salicylaldehyde (3-$OCH_3$-saloH) afforded in

**Table 1** Analytical and physicochemical data for the complexes [Ln(3-$OCH_3$-salo)$_3$]

| Complex a/a | Ln | Yield/% | C/% | H/% | Ln/% | $\mu_{eff/MB}$ | IR bands/$cm^{-1}$ | |
|---|---|---|---|---|---|---|---|---|
| | | | | | | | $\nu$(C=O) | $\nu$(Ln–O) |
| **1** | Pr | 74 | 48.42 (48.48)[a] | 3.52 (3.53) | 23.70 (23.72) | 4.20 | 1625 | 383 |
| **2** | Nd | 75 | 48.21 (48.24) | 3.52 (3.52) | 24.05 (24.15) | 3.75 | 1627 | 384 |
| **3** | Gd | 62 | 47.12 (47.19) | 3.43 (3.44) | 25.72 (25.77) | 9.04 | 1623 | 388 |
| **4** | Dy | 69 | 46.78 (46.80) | 3.41 (3.42) | 26.37 (26.40) | 10.62 | 1624 | 389 |
| **5** | Er | 77 | 46.25 (46.45) | 3.39 (3.40) | 26.95 (26.97) | 9.39 | 1620 | 392 |

[a] Calculated values in parenthesis

good yield very stable in air solid compounds. The characterization of their molecular structure was made by elemental analyses, conductivity and magnetic measurements, as well as by infrared spectroscopy. All the studied complexes are neutral and possess 1:3 metal-to-ligand composition, as it is indicated from elemental analyses and the absence of electrical conductivities ($\sim$3 S $cm^2$ $mol^{-1}$) in DMF solutions. The room temperature magnetic moments ($\mu_{eff}$) are characteristics of trivalent lanthanide ions, showing very close agreement with the theoretical values calculated from Van Vleck formula. Similar values have been observed with substituted benzoate complexes of lanthanides [25]. The complexes may be formulated as [Ln(3-$OCH_3$-salo)$_3$] evidence also arisen from the interpretation of the IR data of the ligand and the complexes. Upon coordination, the bands stemming from the stretching and bending vibrational modes of the phenolic OH (3410 and 1390 $cm^{-1}$) in the free ligand, disappear indicating the removal of the hydrogen atom, while the band at 1641 $cm^{-1}$ attributable to stretching vibration of the C=O bond is shifted to lower frequencies ($\sim$1623 $cm^{-1}$), indicative of their coordination mode [26]. The coordination bond is also inferred from the bands due to the Ln–O at $\sim$388 $cm^{-1}$. Their physicochemical characteristics are listed in Table 1.

## Thermal and kinetic behavior

The temperature ranges, the determined percentage mass losses, and the thermal effects accompanying the decomposition are given in Table 2. Representative thermal curves are depicted for the Pr and Er complexes in Figs. 1 and 2, respectively.

The simultaneous TG and DTA results of the Pr complex are similar as those of the set of complexes Nd, Dy, Gd, and Er. It is obvious that there is no crystallized water or alcohol solvent molecule in the compounds. Both Pr and the set of complexes undergo three-stage decomposition to give the respective oxide as the final products. In the first stage, the complexes 2–5 undergo an endothermic decomposition with $DTG_{max}$ at about 300 °C (Fig. 2). The first derivative of the thermogravimetric curve allows to distinguish the initial release of either one salicylaldehyde molecule(HL), as in the case of the Gd, Dy, and Er complexes, or of the fragment PhO (derived from the salicylaldehyde ligand) as in the case of the Nd complex. The DTA curve shape indicates that no melting takes place before decomposition for these complexes.

For the Pr compound, however, the DTA curve (Fig. 1) shows a sharp endothermic peak at 279 °C, which is seemingly followed by a sharp exothermic at 290 °C. The first peak is attributed to simultaneous melting and decomposition of the compound, as it was evidenced with automated melting point capillary tube system in static air (m.p. at 274–276 °C). The decomposition commences with a sudden mass loss of 15% with $DTG_{max}$ at 290 °C, attributable to the PhO moiety. In order to explain the sharp exothermic peak of the first stage, the same experiment was recorded at a heating rate of 5 °C $min^{-1}$ (Fig. 3). As it is seen from the thermoanalytical curves, the endothermic peak at 275 °C is followed from a rather broad and with smaller heat flow value exothermic peak at 283 °C, suggesting that it could be regarded as a continuation of the endothermic one and that the first stage is accompanied by an endothermic decomposition along with the melting of the Pr compound.

Upon increasing the temperature, the unstable intermediates undergo further decomposition (at $\sim$390 or 400 °C) with mass loss attributable to the elimination of carbon monoxide plus the methoxy moiety for all the complexes. This second degradation stage is accompanied by an exothermic thermal effect as it is evidenced from the DTA curve, which is maybe due to the rapid elimination of the gaseous decomposition products (as it happens to explosions) or to partially oxidation of the released carbon monoxide to carbon dioxide. Efforts to isolate the intermediates were not successful due to their continuous decomposition, as it was evidenced from the TG curves.

The third degradation stage follows beyond 470 °C until 1000 °C, with a continuous mass loss, possibly attributable to successive elimination of the second and third ligands. The smaller quantities found may be considered as

**Table 2** Thermoanalytical results (TG/DTG–DTA) for the complexes [Ln(3-$OCH_3$-salo)$_3$] in nitrogen

| a/a | Stage | $T_{range}$/°C | Evolved moiety formula | DTGmax/°C | DTA/°C | Mass loss exp/% (mass loss calc/%) |
|---|---|---|---|---|---|---|
| **1** | I | 250–330 | PhO | 290 | 279(−) | 15.0 (15.65) |
| | II | 330–470 | {CO + $OCH_3$} | 390 | 390(+) | 10.2 (4.71 + 5.22) |
| | III | 470–1000 | 2{L–O} | – | 640(+), 780(+), 820(+) | 24.0 + *x* (45.44) |
| | Residue | >950 | Mixture of (Pr2O3, Pr6O11) + C | | | 49.7 (27.78, 28.67 + *x*) |
| **2** | I | 250–340 | PhO | 295 | 295(−) | 16.3 (15.58) |
| | II | 340-470 | {CO + $OCH_3$} | 380 | 380(+) | 10.0 (4.69 + 5.19) |
| | III | 470–1000 | 2{L–O} | – | 600(+), 750(+), 850(+) | 19.0 + *x* (45.22) |
| | Residue | >950 | $Nd_2O_3$ + C | | | 55.0 (28.14 + *x*) |
| **3** | I | 280–340 | HL | 300 | 300(−) | 25.0 (24.92) |
| | II | 340–470 | {CO + $OCH_3$} | 385 | 385(+) | 10.0 (4.59 + 5.08) |
| | IIIa | 470–800 | PhO | 680 | 720(+) | 15.0 (15.24) |
| | b | 800–1000 | Unknown | – | 850(+) | 8.0 |
| | Residue | >980 | $Gd_2O_3$ + C | | | 42.0 (29.67 + *x*) |
| **4** | I | 285–350 | HL | 305 | 305(−) | 24.7 (24.69) |
| | II | 350–500 | {CO + $OCH_3$} | 400 | 400(+) | 9.9 (4.55 + 5.04) |
| | III | 500–1000 | Unknown (or PhO) | 680 | 680(+) | 13.4 (15.11) |
| | Residue | >980 | $Dy_2O_3$ + C | | | 52.0 (30.30 + x) |
| **5** | I | 285-340 | HL | 310 | 310(−) | 24.8 (24.52) |
| | II | 340–490 | {CO + $OCH_3$} | 420 | 420(+) | 10.0 (4.52 + 5.00) |
| | III | 490–1000 | Unknown (or PhO) | 680 | 720(+), 840(+) | 15.0 (15.0) |
| | Residue | >980 | $Er_2O_3$ + C | | | 50.2 (30.80 + *x*) |

*x* non-combusted carbon, (−) endothermic thermal effect, (+) exothermic

PhO = $C_6H_5O$, HL = 3-$OCH_3$-salicylaldehyde ligand, L–O = ligand–oxygen

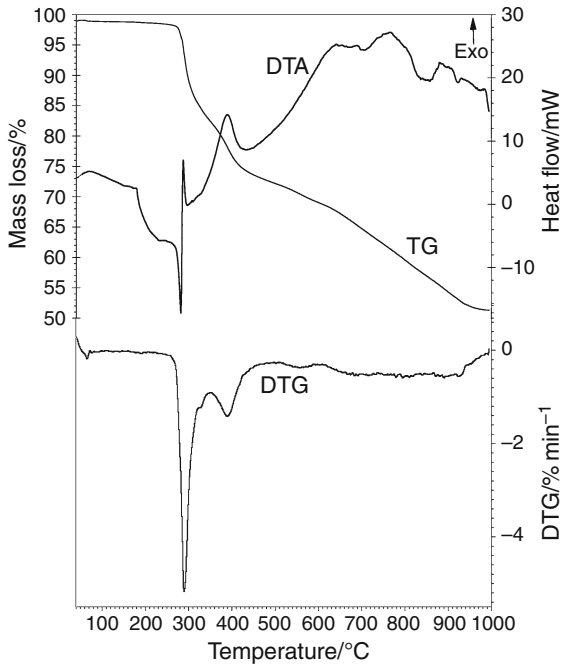


**Fig. 1** Thermoanalytical curves (TG/DTG–DTA) of Pr (**1**) complex in nitrogen. Heating rate 10 °C $min^{-1}$

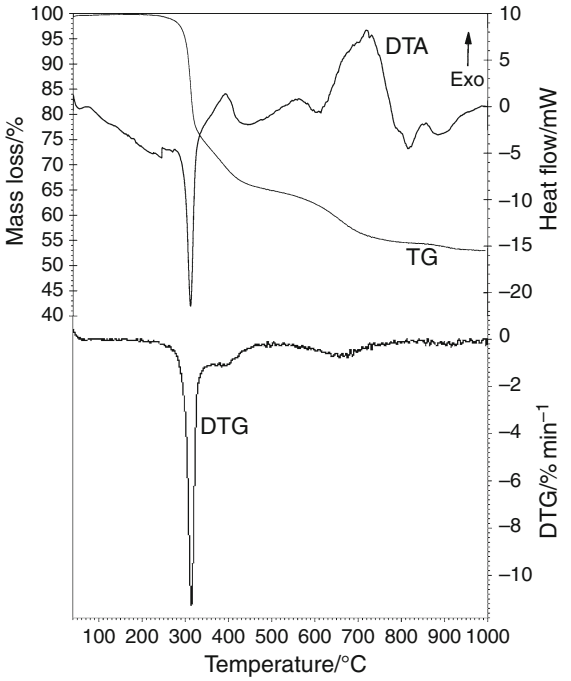


**Fig. 2** Thermoanalytical curves (TG/DTG–DTA) of Er (**5**) complex in nitrogen. Heating rate 10 °C $min^{-1}$

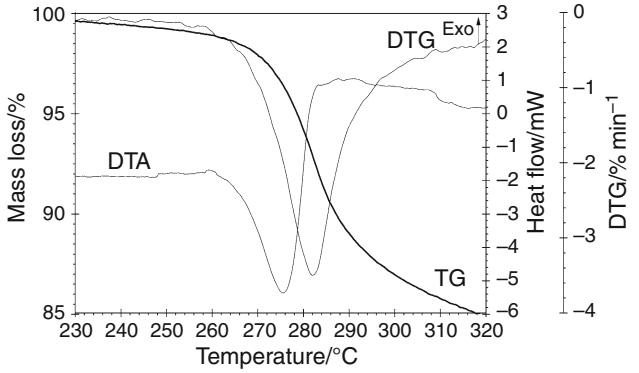


**Fig. 3** Thermoanalytical curves (TG/DTG–DTA) for the first decomposition stage of Pr (**1**) complex in nitrogen. Heating rate 5 °C $min^{-1}$

non-combustible residues of the organic fragments of the compounds. This speculation can be enhanced from the composition of the final residues. The residues at 1000 °C for all the studied complexes are carbonaceous solids consisting of the respective lanthanide oxide $Ln_2O_3$ plus carbon in a ratio of ~20% of the complex, evidence arisen from the TG/DTG curves and IR peak at ~385 $cm^{-1}$, attributable to Ln–O bond, in agreement with other analogous lanthanide compounds [27]**.** The formation of the oxides $Ln_2O_3$ was observed at ~750 °C as it was expected [28]. Powder XRD diagrams for the final residue of all the complexes are given in Fig. 4, confirming the existence of the lanthanide oxide as $Ln_2O_3$. When the purging flow is changed to static air the obtained residues at 1000 °C were pure oxides without carbon content. An example is given for the praseodymium complex at heating rate 20 °C $min^{-1}$ (Fig. 5). The experimental total mass loss of the thermal decomposition 70% collaborates with the expected residue $Pr_6O_{11}$ (calculated 28.7%), evidence arisen from its XRD diagram (Fig. 6).

By the analysis of the evolved gases, performed by online coupling a MS spectrometer to the thermobalance, the proposed decomposition stage can be confirmed. Examination of the ionic current profiles during decomposition in inert, under nitrogen or argon atmosphere of the investigated compounds has shown the presence of small molecules, released at the 280–350 and 350–500 °C temperature ranges, which correspond to the decomposition stages I and II, respectively.

As seen in the MS spectra of the thermal decomposition released gases of the erbium complex, given as an example in Fig. 7, the detected masses for the first stage with m/z: 30, 32, and 44 are assigned to formaldehyde ($H_2CO$), methanol ($CH_3OH$), and carbon dioxide ($CO_2$), respectively. For the second stage, the masses m/z: 18, 28, and 44 are assigned to water vapor ($H_2O$), carbon monoxide (CO), and carbon dioxide ($CO_2$), respectively. The existence of the carbon dioxide explains the exothermic nature of the

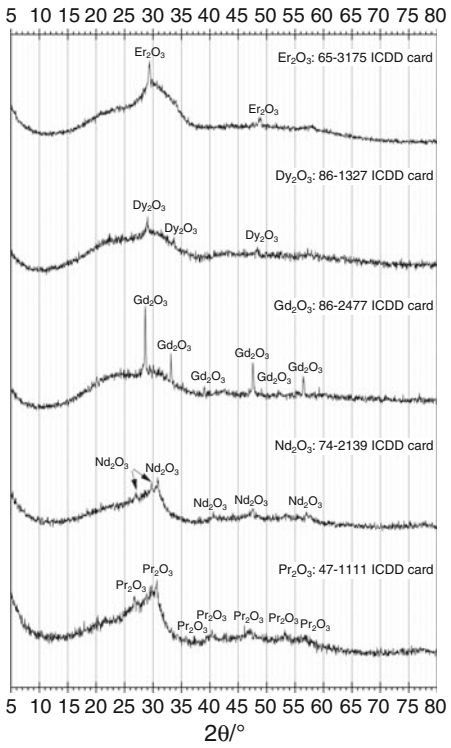


**Fig. 4** Powder XRD for the thermal decomposition residues in nitrogen of the lanthanide complexes at 1000 °C

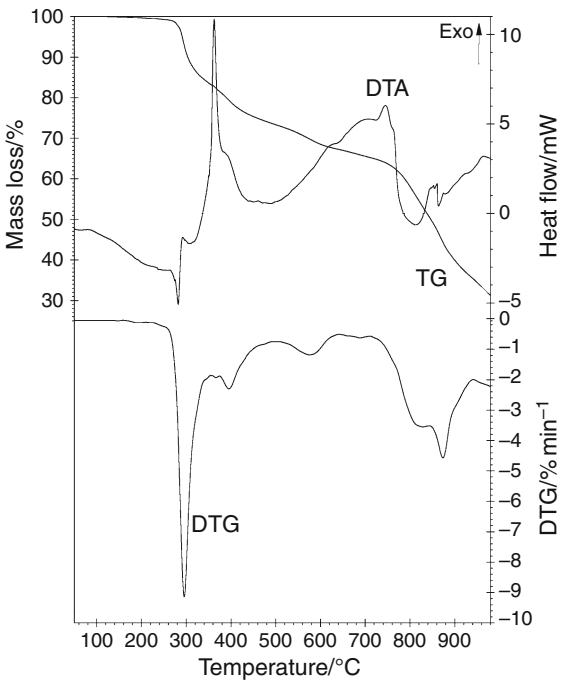


**Fig. 5** Thermoanalytical curves (TG/DTG–DTA) of Pr (**1**) complex in static air. Heating rate 20 °C $min^{-1}$

second decomposition, possibly due to the oxidation of the released carbon monoxide. All the detected ions derived from the fragmentation of the 3-methoxy-salicylaldehyde

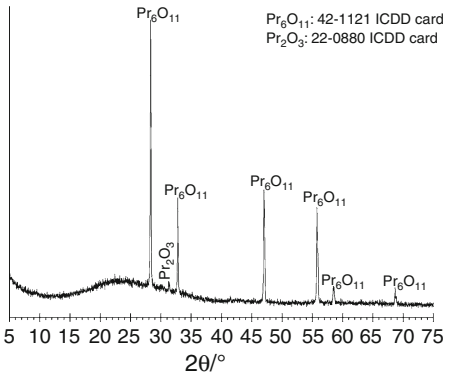


**Fig. 6** Powder XRD for the thermal decomposition residue in static air of the Pr complex at 1000 °C

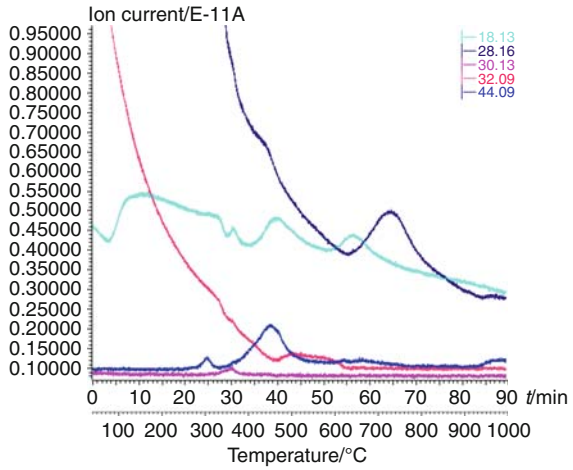


**Fig. 7** Ionic current profiles recorded during TG–MS analysis of the Er complex (**5**) in argon atmosphere

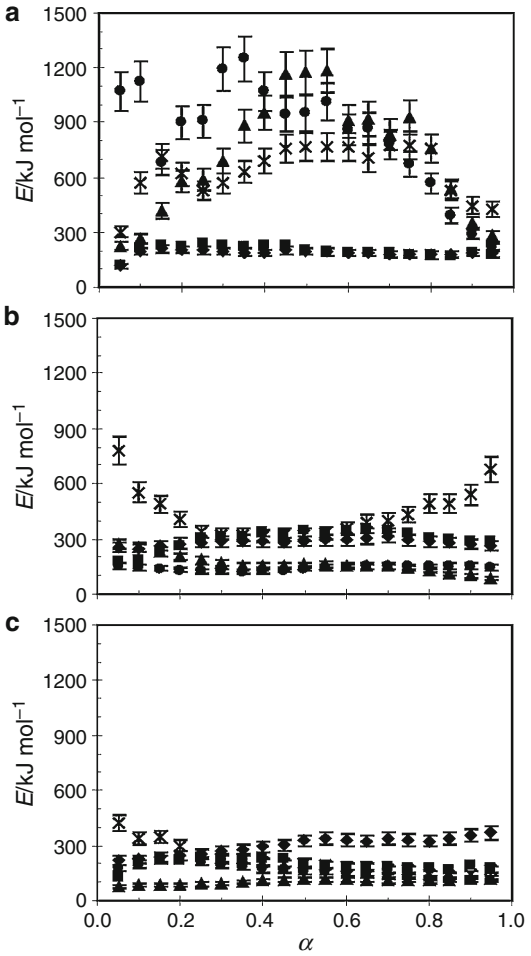


**Fig. 8** Conversion dependence of activation energy for thermal decomposition processes: **a** first stage, **b** second stage, and **c** third stage. *Filled square*—$PrL_3$, *filled diamond*—$NdL_3$, *filled triangle*—$GdL_3$, *filled circle*—$DyL_3$, and *cross*—$ErL_3$

ligand (molecular ion 152), so confirmed the proposed fragmentation pattern by the mass loss on the TG/DTG curves. At the third stage, beyond 490 °C the detected masses (m/z: 18, 32, and mainly 28) are again fragments of the ligand.

The analysis of thermal behavior enable to conclude that the lanthanide (III) complexes (**1**–**5**) are stable, showing a TG plateau, up to at least 250 °C, when the break-down starts. The stability of the complexes examined can be assessed according to the thermal profile recorded in nitrogen atmosphere. The *onset decomposition temperatures* (Table 2) indicate that the thermal stability of the studied lanthanide complexes follows the series: $ErL_3 \approx DyL_3 > GdL_3 > Nd \approx Pr$.

The kinetic analysis of the first three decomposition stages by isoconversional OFW method provides a conversion dependence of activation energy for each decomposition stage. The results are summarized in Fig. 8a–c for the first, second, and third decomposition stages, respectively.

As far as the first stage is concerned (plot a), noticeably (and only partially realistic) higher and variable $E$ values can be observed for Er(III), Dy(III), and Gd(III) complexes substantially confirming the stability order previously assessed. Furthermore, the remarkable high $E$ values and their significant variation (about 600–700 kJ mol$^{-1}$) related to the first stage of these complexes can be partially ascribable to an artifact, but is unquestionably be explained by the negligible shift of the TG curves toward higher temperatures with increasing the heating rate. Lower, more reasonable and comparable $E$ values are calculated for the first stage of Nd(III) and Pr(III), in agreement with the stability scale based on decomposition temperature. The highest activation energies related to the second and third stages (plots b and c) are those of the Er(III) complex, whose variation demonstrates the complex nature of decomposition processes and the need to use more than one method for a more complete kinetic characterization.

**Table 3** Regression and kinetic parameters for the decomposition processes obtained by the Kissinger method

| Complexes | Stage | $\ln(\beta/T_m^2) = a' + b' \cdot (T_m^{-1})$ | | $R^2$ | $E$/kJ mol$^{-1}$ | $\ln(A/\text{min}^{-1})$ | $-\ln(k/\text{min}^{-1})$[a] |
|---|---|---|---|---|---|---|---|
| | | $a'$ | $b'$/K | | | | |
| $[Pr(L)_3]$ | I | 31 ± 3 | –23 ± 2 | 0.9899 | 194 ± 14 | 41 ± 3 | –0.3 (562 K) |
| | II | 42 ± 4 | –35 ± 3 | 0.9860 | 293 ± 25 | 53 ± 4 | –0.2 (664 K) |
| | III | 35 ± 4 | –39 ± 3 | 0.9858 | 321 ± 27 | 46 ± 4 | –0.5 (831 K) |
| $[Nd(L)_3]$ | I | 30 ± 4 | –22 ± 3 | 0.9905 | 185 ± 25 | 40 ± 4 | –0.3 (563 K) |
| | II | 41 ± 3 | –34 ± 3 | 0.9855 | 284 ± 25 | 52 ± 3 | –0.4 (664 K) |
| | III | 36 ± 4 | –39 ± 3 | 0.9876 | 328 ± 25 | 47 ± 4 | –0.4 (832 K) |
| $[Gd(L)_3]$ | I | 302 ± 7 | –180 ± 4 | 0.9987 | 1500 ± 35 | 310 ± 7 | –1.5 (576 K) |
| | II | 71 ± 9 | –54 ± 6 | 0.9770 | 453 ± 50 | 82 ± 9 | –0.3 (669 K) |
| | III | 15 ± 3 | –25 ± 3 | 0.9782 | 211 ± 3 | 25 ± 3 | 1.2 (935 K) |
| $[Dy(L)_3]$ | I | 201 ± 7 | –123 ± 4 | 0.9988 | 1030 ± 40 | 213 ± 7 | –1.2 (582 K) |
| | II | 29 ± 2 | –26 ± 1 | 0.9961 | 218 ± 10 | 39 ± 2 | 0.5 (666 K) |
| | III | 14 ± 1 | –23 ± 1 | 0.9989 | 194 ± 5 | 24 ± 1 | 1.3 (935 K) |
| $[Er(L)_3]$ | I | 320 ± 30 | –193 ± 19 | 0.9814 | 1610 ± 150 | 330 ± 30 | –1.7 (585 K) |
| | II | 24 ± 5 | –23 ± 3 | 0.9584 | 190 ± 30 | 34 ± 5 | 0.6 (668 K) |
| | III | 21 ± 3 | –30 ± 2 | 0.9859 | 250 ± 20 | 31 ± 3 | 1.0 (940 K) |

The associated uncertainty is standard deviations

$L$ the anion of the 3-$OCH_3$-salicylaldehyde ligand

[a] Calculated at the mean of experimental temperature range indicated in parentheses

Activation energies, pre-exponential factors, and rate constant $k$ (calculated at the mean of the respective temperature ranges) obtained by the Kissinger method are given in Table 3.

In the last column on the right the decreasing values of $-\ln k$ (mainly the values related to the first stage) can provide a more reliable decreasing stability order. Taking into account this assumption, the lower values (which identify the faster process) can be found for the first stage regardless which complex is considered (only slight differences are observed). For the Er(III), Dy(III), and Gd(III) complexes the third stage seems to be the rate-determining stage, while for Pr(III) and Nd(III) complexes no significant differences are found by comparing the rate constant values of the three stages. By considering the $-\ln k$ values related to the third stage, the comparable higher stability can be attributed to Er(III), Dy(III), and Gd(III) complexes and the comparable lower stability to Pr(III) and Nd(III) complexes.

These conclusions are in substantial agreement with the results derived by considering the decomposition temperature and partially agree with the results obtained by considering the thermal decomposition of another series of lanthanide(III) complexes taken from literature [19], whose $-\ln k$ values were calculated from the Arrhenius parameters for the slower decomposition stage:

$$\text{Gd(III)} \gg \text{Er(III)} > \text{Dy(III)} \sim \text{Nd(III)} \sim \text{Pr(III)}$$

## Conclusions

From the obtained results it appears that the lanthanide(III) complexes with the ligand 3-methoxy-salicylaldehyde were synthesized as neutral complexes. The ligand behaves as bidentate chelating agent in its mono-anionic form. The complexes upon heating up to 1000 °C in inert atmosphere decompose in three stages leaving as final residue carbonaceous oxides of $Ln_2O_3$, proved by powder XRD measurements. On heating the Pr complex in static air up to 1000 °C, the $Pr_6O_{11}$ oxide was obtained as final residue, proved by powder XRD.

The released decomposition gases, analyzed by coupled MS spectrometer to the thermobalance, were found to be small fragments of the ligand at specific temperatures, proved the proposed decomposition stages. Kinetic analysis of decomposition processes performed in these lanthanide(III) complexes confirms that thermal decomposition has usually a complex nature. Also, it is possible to assess a stability scale in a more reliable way by comparing the rate constant values, which compensate enthalpic and entropic stability contributions of activation energy and pre-exponential factor, respectively.

## References

1. Nishikido J, Kamishima M, Matsuzawa H, Mikami K. Recyclable Lewis acid catalysis by tuning supercritical vs liquid carbon dioxide

phases: lanthanide catalysts withtris(perfluorooctanesulfonyl)methide and bis(perfluorooctanesulfenyl)amide. Tetrahedron. 2002;58(41):8345–9.
2. Louie A, Huber M, Ahreus E, Rothbacher U, Moats R, Jacobs R, et al. In vivo visualization of gene expression using magnetic resonance imaging. Nat Biotechnol. 2000;18(3):321–5.
3. Reisfeld R, Jorgensen C. Laser and excited states of rare earths. Berlin: Springer; 1977.
4. Cotton F, Wilkinson G, Murillo C, Bochman M. Advanced Inorganic Chemistry. 6th ed. New York: Willey; 1999. p. 11.
5. Prasad RN, Agrawal A. Synthesis and spectroscopic studies of mixed ligand complexes of cobalt(II) with salicylaldehyde, hydroxyarylketones and beta-diketones. J Indian Chem Soc. 2006;83(1):75–7.
6. Fujinaga K, Sakaguchi Y, Tsuruhara T, Seike Y, Okumura M. Solvent extraction of transition metal ions by an in situ extractant formation method: salicylaldoxime forming system. Solvent Extr Res Dev. 2001;8:144–58.
7. Sun Y-X, Gao G-Z. bis(4-Bromo-2-formylphenolato-$\kappa^2$ O,O′)copper(II). Acta Cryst. 2005;E61(2):m354–5.
8. Yang Y-M, Lu P-C, Zhu T-T, Liu C-H. bis(2-Formylphenolato-$\kappa^2$ O,O′)iron(II). Acta Cryst. 2007;E63(6):m1613.
9. Pessoa JC, Cavaco I, Correira I, Tomaz I, Duarte T, Matias PM. Oxovanadium(IV) complexes with aromatic aldehydes. J Inorg Biochem. 2000;80(1):35–9.
10. Lalia-Kantouri M, Papadopoulos CD, Hatzidimitriou AG, Skoulika S. Hetero-heptanuclear (Fe–Na) complexes of salicylaldehydes: crystal and molecular structure of $[Fe_2(3\text{-}OCH_3\text{-salo})_8/Na_5]\cdot 3OH\cdot 8H_2O$. Struct Chem. 2009;20:177–84.
11. Lalia-Kantouri M, Dimitriadis T, Papadopoulos CD, Gdaniec M, Czapik A, Hatzidimitriou AG. Synthesis and structural characterization of Iron(III) complexes with 2-Hydroxyphenones. Z Anorg Allgem Chem. 2009;635:2185–90. doi:10.1002/zaac.20090016.
12. Lopes WS, Morais CRS, Souza AG, Leite VD, de A Firmo BD. Study of isothermal decomposition of lanthanide mixed complexes with 2,2,6,6-tetramethyl-3,5-heptanodione and 1,10-phenqanthroline. J Therm Anal Calorim. 2007;87(3):841–5.
13. Ferenc W, Dziewulska-Kulaczkowska A, Sarzynski J, Paszkowska B. 4-Chloro-2-methoxybenzoates of heavy lanthanides(III) and yttrium(III). Thermal, spectral and magnetic behaviour. J Therm Anal Calorim. 2008;91(1):285–92.
14. Premkumar T, Govindarajan S. Thermoanalytical and spectroscopic studies on hydrazinium lighter lanthanide complexes of 2-pyrazinecarboxylic acid. J Therm Anal Calorim. 2009;74:325–33. doi:10.1007/s10973-009-0117-1.
15. Hangming G. Synthesis, characterization and thermal analysis of lanthanide(III) nitrates complexes of Schiff base derived from *o*-vanilline and *p*-toluidine. Asian J Chem. 2009;21(2):1113–8.
16. Lalia-Kantouri M, Papadopoulos CD. Thermal investigation by simultaneous TG/DTG-DTA and IR spectroscopy of new lanthanide complexes with salicylhydroxamic acid. J Therm Anal Calorim. 2005;81:375–80.
17. Lalia-Kantouri M, Tzavellas L, Paschalidis D. Novel Lanthanide complexes with di-2-pyridylketone-p-chloro-benzoylhydrazine. Thermal investigation by simultaneous TG/DTG-DTA and IR spectroscopy. J Therm Anal Calorim. 2008;91(3):937–42.
18. Vinodkumar CR, Muraleedharan Nair MK, Radhakrishnan PK. Thermal studies on lanthanide nitrate complexes of 4-*n*-(2′-furfurylidene)aminoantipyrine. J Therm Anal Calorim. 2000;61(1):143–9.
19. Muraleedharan Nair MK, Radhakrishnan PK. Thermal decomposition kinetics and mechanism of lanthanide perchlorate complexes of 4-*N*-(4′-antipyryl-methylidene) aminoantipyrine. Thermochim Acta. 1997;292(1–2):115–22.
20. Lyle S, Rahman M. Complexometric titration of yttrium and the lanthanons I: a comparison of direct methods. Talanta. 1963;10(1):1177–82.
21. Flynn JH, Wall LA. A quick direct method for the determination of activation energy from thermogravimetric data. J Polym Sci B: Polym Lett. 1966;4(5):323–8.
22. Ozawa T. A new method of analyzing thermogravimetric data. Bull Chem Soc Jpn. 1965;38:1881–6.
23. Doyle CD. Estimating isothermal life from thermogravimetric data. J Appl Polym Sci. 1962;6(24):639–42.
24. Kissinger HE. Reaction kinetics in differential thermal analysis. Anal Chem. 1957;29(11):1702–6.
25. Ferenc W, Walkow-Dziewulska A, Bocian B. Thermal and spectral studies of 2,4,5-trimethoxybenzoates of heavy lanthanides(III) and yttrium(III). J Therm Anal Calorim. 2005;79(1):145–50.
26. Nakamoto K. Infrared and Raman spectra of inorganic and coordination compounds. Toronto: Wiley; 1997.
27. Sivasankar BN, Sharmila JR. Thermal and spectral properties of some anhydrous and hydrated rare earth hydrazine carboxylates. J Therm Anal Calorim. 2003;73(1):271–83.
28. Duval C. Inorganic thermogravimetric analysis. 2nd and Revised ed. Amsterdam: Elsevier; 1963. p. 547–663.